ANNUAL REVIEWS

Annual Review of Materials Research

Grain Boundary Migration in Polycrystals

Gregory S. Rohrer,[1] Ian Chesser,[2] Amanda R. Krause,[1] S. Kiana Naghibzadeh,[3] Zipeng Xu,[1] Kaushik Dayal,[3] and Elizabeth A. Holm[4]

[1]Department of Materials Science and Engineering, Carnegie Mellon University, Pittsburgh, Pennsylvania, USA; email: gr20@andrew.cmu.edu, amandakr@andrew.cmu.edu, zipengx@andrew.cmu.edu

[2]Department of Physics and Astronomy, George Mason University, Fairfax, Virginia, USA; email: ichesser@gmu.edu

[3]Department of Civil and Environmental Engineering, Carnegie Mellon University, Pittsburgh, Pennsylvania, USA; email: snaghibz@andrew.cmu.edu, kaushik.dayal@cmu.edu

[4]Department of Materials Science and Engineering, University of Michigan, Ann Arbor, Michigan, USA; email: eaholm@umich.edu

Annu. Rev. Mater. Res. 2023. 53:347–69

First published as a Review in Advance on February 28, 2023

The *Annual Review of Materials Research* is online at matsci.annualreviews.org

https://doi.org/10.1146/annurev-matsci-080921-091511

Keywords

grain boundary, microstructure, grain growth, grain boundary migration

Abstract

Grain boundaries in polycrystalline materials migrate to reduce the total excess energy. It has recently been found that the factors governing migration rates of boundaries in bicrystals are insufficient to explain boundary migration in polycrystals. We first review our current understanding of the atomistic mechanisms of grain boundary migration based on simulations and high-resolution transmission electron microscopy observations. We then review our current understanding at the continuum scale based on simulations and observations using high-energy diffraction microscopy. We conclude that detailed comparisons of experimental observations with atomistic simulations of migration in polycrystals (rather than bicrystals) are required to better understand the mechanisms of grain boundary migration, that the driving force for grain boundary migration in polycrystals must include factors other than curvature, and that current simulations of grain growth are insufficient for reproducing experimental observations, possibly because of an inadequate representation of the driving force.

1. INTRODUCTION

Grain boundary (GB) migration is the mechanism by which polycrystalline microstructures evolve in metals, ceramics, polymers, and rocks. Because GB migration changes the average crystal size, it also influences the electrical, optical, and mechanical properties of the material. Materials scientists have, therefore, attempted to control GB migration and grain size. As examples, near-single crystal structures can be produced from powders in the solid state by facilitating GB migration (1), and stable nanocrystalline structures can be produced by impeding migration (2).

The topic of GB migration has been reviewed in the past (3–6), with the most authoritative and comprehensive source being Gottstein & Shvindlerman's book (7). However, the most recent review is now more than 10 years old. Since that time, there have been some remarkable developments. The first is that it is now possible to directly observe GB migration in 3D polycrystalline metals and ceramics using high-energy diffraction microscopy (HEDM) (8) or diffraction contrast tomography (DCT) (9). A second important development is the availability of growing amounts of GB energy data, from both experiment and simulation (10). GB properties such as the GB energy have five degrees of freedom describing bicrystal geometry. Therefore, determining GB energies over the parameter space required large-scale automated measurements and calculations that have been mastered only recently. Knowledge of these properties makes it possible to move beyond the traditional assumption of uniform GB properties. A third important development is the formulation of a theory for defect-mediated GB migration (11). The theory is based on the idea that the rates of GB migration are controlled by the nucleation, glide, and climb of GB disconnections. This mechanism has the potential to explain the anisotropy of GB migration rates and some puzzling phenomena such as GB stagnation.

Rather than being comprehensive, the current review is focused on recent developments and GB migration driven by the reduction in the overall GB excess energy. We do not consider migration driven by stored plastic energy or chemical driving forces, nor by electric, magnetic, and thermal driving forces, except in cases where results based on capillarity are unavailable [this is the case for many atomistic simulations, high-resolution transmission electron microscopy (HRTEM) studies, and some bicrystal studies]. The review is organized in the following way. In Section 2 we consider atomistic mechanisms of GB migration based on the results of simulations and experiments. In Section 3 we review our understanding of GB migration at the continuum scale, again comparing this to the results of simulations and experiments. The review concludes with a summary of current knowledge and suggestions for future research directions.

2. ATOMISTIC PHENOMENA IN GRAIN BOUNDARY MIGRATION

2.1. Grain Boundary Migration Mechanisms

There are three prevailing models for GB migration that are described below. The first is based on the assumption that atoms transfer from one crystal to another by surmounting an activation barrier, the second is that grains in polycrystals grow by the same mechanism that they grow in a liquid or vapor, and the third is that their migration is defect mediated.

2.1.1. Rate theory model for grain boundary migration. The classical theory for GB migration assumes that migration velocity (v) is proportional to the driving force [the product of the mean curvature ($\boldsymbol{\kappa}$) and GB energy (γ)],

$$v = M\boldsymbol{\kappa}\gamma, \qquad 1.$$

where the constant of proportionality is the GB mobility (M) (12, 13). The mobility has traditionally been modeled as a scalar quantity related to the thermally activated atom transfer from one

crystal orientation to another,

$$M = M_0 e^{\frac{-H_a}{k_b T}}, \qquad 2.$$

where M_0 is an entropic prefactor, H_a is the activation energy, and $k_b T$ is the thermal energy. Because Equation 2 fits the majority of experimental data to a high degree of accuracy (4), little effort was made to add complexity to this model.

There are, however, notable examples where Equations 1 and 2 fail to describe observations. For example, the observation of cryogenic and thermally damped GB migration (14) and antithermal GB migration (15) cannot be explained by Equation 2. It has recently been pointed out that Equation 2 applies only in the condition that $H_a \gg \kappa\gamma$, and when the barrier is small compared with the driving force, both cryogenic and thermally damped GB migration are possible (16). Recent experimental (17–19) and computational (11, 20–22) studies also draw into question the validity of Equation 1, which does not agree with observations in polycrystals. In summary, while the simple model depicted by Equations 1 and 2 is consistent with observations of bicrystals and some average behavior of polycrystals, it has not been successful in describing the motion of individual boundaries in polycrystals.

2.1.2. The terrace-ledge-kink model for grain boundary migration. The first step beyond the simple concept of transferring atoms across a boundary was proposed by Gleiter (3, 23), who assumed that GB migration occurs by a mechanism analogous to crystal growth. Specifically, based on transmission electron microscopy (TEM) observations, the two adjacent grain surfaces were taken to be terrace-ledge-kink structures, and the rate of migration was assumed to be controlled by the emission of atoms from the steps on one surface and the absorption of these atoms onto steps on the other surface, with continuous step sources provided by screw dislocations intersecting the GB plane. This is the first model that leads to a GB migration velocity that depends on the crystallography of the boundary (3), which is a well-known characteristic of GB migration (24). Therefore, Gleiter's model can be viewed as the forerunner of contemporary models of boundary migration based on disconnections (described in the next section), which describe both the step structure of the interface and the dislocation content.

2.1.3. The disconnection model for grain boundary migration. Disconnections are line defects at interfaces with step and/or dislocation components (25, 26). Although the existence of disconnections has long been known within the interface community, recent efforts have been made to augment the traditional picture of GB migration with a microscopic model based on the nucleation and migration of competing disconnection modes (different disconnection modes have different step–Burgers vector combinations in the same GB) (11, 22, 27, 28). This model is significant because of its ability to account for anisotropic GB motion, competing mechanisms, and constraints during grain growth.

Distinct disconnection modes may coexist and compete within the same GB at finite temperature (22). A countable infinite set of disconnection modes with distinct Burgers vectors and step heights ($\mathbf{b}_i$,h_i) can be enumerated for the same GB solely from consideration of macroscopic GB geometry. Geometric enumeration algorithms for disconnection modes in general GBs have recently been developed using mathematical tools from bicrystallography (29). **Figure 1** demonstrates the construction of a disconnection with finite $\mathbf{b}$ and h at an asymmetric GB. This disconnection can advance the boundary only by climb.

One of the simplest manifestations of the disconnection model is a model for the homogeneous nucleation and glide of a single disconnection dipole with character ($\mathbf{b}$,h) from an initially flat quasi-2D GB in a bicrystal (27). Assuming periodic boundary conditions along the interface plane,

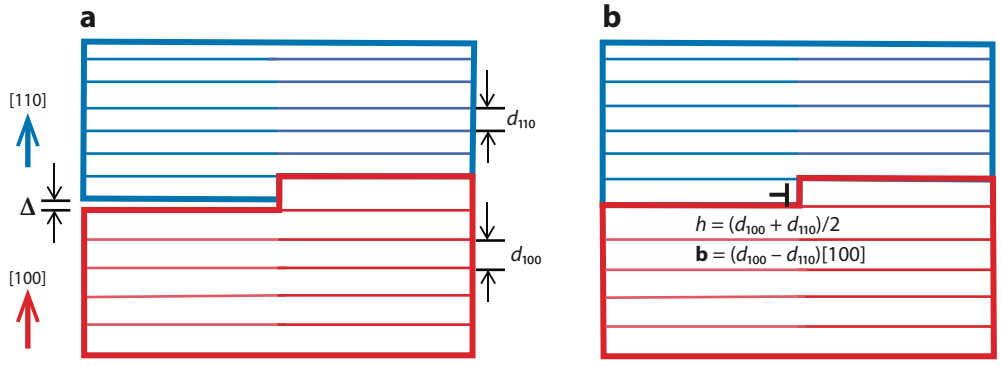

Figure 1

Construction of a disconnection from an asymmetric grain boundary (GB) in a cubic crystal. (*a*) A step is introduced to the interface, leading to a gap of spacing $\Delta = d_{100} - d_{110}$. (*b*) A disconnection is shown, which accommodates the incompatible spacing. This disconnection can move only by climb (Burgers vector normal to the GB plane) and therefore requires diffusion to migrate.

the total energy barrier for migration of a GB from an initial to a final position can be expressed as a sum of three contributions,

$$E_{\text{tot}} = E_{\text{c}} + E_{\text{e}} + E_{\text{m}} = A\,|h| + Cb^2 + E_{\text{m}}, \qquad 3.$$

where E_{c} is a core energy term containing the step and dislocation energy, E_{e} is an elastic interaction energy term arising from interactions between individual dislocations, and E_{m} is a Peierls-like migration barrier for propagation of the disconnection steps along the interface that contains a contribution from atomic slip and shuffling. The total energy barrier for migration, depicted in **Figure 2**, is postulated to be proportional to the sum of the disconnection step height and squared Burgers vector with two fitting parameters, A and C, which contain material- and GB-dependent

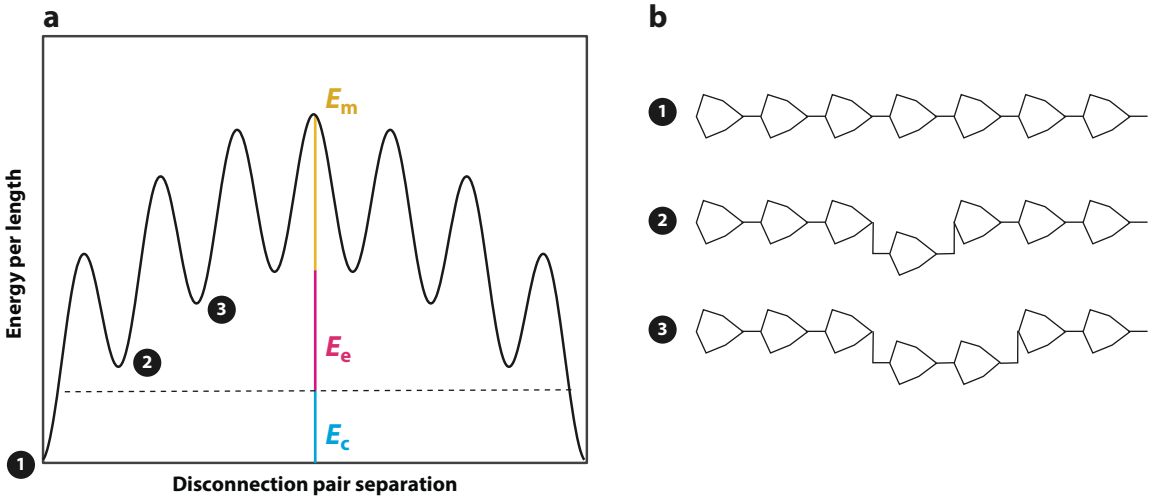

Figure 2

(*a*) A simplified potential energy landscape for disconnection-mediated grain boundary (GB) migration in a quasi-2D flat symmetric GB with periodic boundary conditions. The core energy E_{c}, elastic energy E_{e}, and migration energy E_{m} contribute to the total disconnection nucleation energy barrier. (*b*) GB migration at several points (❶–❸) is illustrated schematically in a GB with kite-shaped structural units.

parameters. The total energy barrier can be computed from atomistic simulations with no fitting parameters, though the full calculation has been performed only for several symmetric tilt GBs in face-centered cubic (FCC) metals (27, 30, 31). These calculations demonstrate that different GBs have distinct disconnection nucleation barrier spectra (values of E_{tot} for the different disconnection modes) and also show that the Peierls-like energy barrier term E_m for disconnection migration varies strongly with GB geometry and cannot be neglected. The disconnection nucleation model, even for nominally flat GBs in bicrystals, is still in need of parametrization and testing for a wide range of GB and material types.

Two distinct driving force terms are discussed in the disconnection literature: an energy jump driving force that couples to the step component of a disconnection and a stress driving force that couples to the Burgers vector component. On this basis, mobility is argued to be best expressed as a tensor relating normal and sliding velocity to energy jump and stress driving forces (32). Types of predictions that can be made from the disconnection model include the temperature and driving force dependence of the coupling factor and mobility (27, 33). The predictions of mobility and coupling factor in the work of Srolovitz and coworkers (27, 33) are self-consistent with molecular dynamics (MD) simulations up to the fitting parameters in the nucleation model (27). Once again, however, these theoretical considerations and simulations have been applied to only a handful of symmetric GBs.

When a GB is curved and attached to other GBs as part of a network, it adds complications to the disconnection nucleation model that have not been completely resolved. Dislocation content is not conserved during curved GB migration (34), and disconnection nucleation or annihilation is required for growing or shrinking grains. Triple junction (TJ) migration likewise requires disconnection annihilation reactions at the TJ in appropriate combinations to avoid the build-up of large residual stresses associated with dislocation pile-ups (28). Annihilation that releases built-up stress might be the cause of observed abrupt motion, as described in Section 2.3. An important theme from recent disconnection-based work is that multiple mechanisms are required to relax stresses during polycrystalline grain growth, including the formation of annealing twins and the activation of secondary disconnection modes (22, 28, 35). From the perspective of disconnection nucleation energy spectra, GBs with large flexibility of motion in polycrystals are expected to have either an available low-energy mode with no dislocation character (as in many twist or general GBs) or multiple low-energy modes available that can accommodate the shape change required for GB motion without the generation of significant shear stress. A small fraction of slow GBs or TJs may contribute to grain growth stagnation (21, 28, 36).

2.2. Atomistic Simulations of Grain Boundary Migration

Atomistic simulations have contributed significantly to our understanding of GB migration mechanisms. The majority of atomistic GB migration studies have been conducted via classical MD simulations of pure metals with semiempirical interatomic potentials, grain sizes rarely exceeding 10 nm, and timescales of migration rarely exceeding 10 ns. While simulations and experiments agree reasonably on some fronts, such as GB energy anisotropy in pure materials (10, 37, 38) and coupling factors in symmetric bicrystals (39), some simulation results are unconfirmed, appear to be at odds with experiments, or are outside of the domain of current experimental measurements. In this section, we review recent scientific insights gained from atomistic simulations of GB migration and highlight several outstanding challenges.

Much of the disconnection model has been developed around discoveries from MD simulations in bicrystals and polycrystals. Seminal MD work from Cahn et al. (40) showed that coupling factors of symmetric tilt GBs in bicrystals follow well-defined geometric branches as a function of

misorientation angle. These branches have been confirmed in bicrystal experiments, and this active area of research was reviewed by Molodov & Molodov (39). Curved GBs in cylindrical bicrystals with special misorientation axes have also been predicted to show the shear coupling effect via grain rotation during shrinkage (34, 41). This effect was recently observed in a 2D material (42).

It is noteworthy that during polycrystalline grain growth, no significant grain rotation is observed. What are the mechanisms by which grains in a polycrystal conspire to move with zero net coupling factor? When flat and cylindrical bicrystal motion are constrained in MD simulations, shear coupling factors are observed to disappear (22, 34) if migration does not stagnate and if they were not already zero in the unconstrained system. One possible origin of this behavior is that different disconnection modes can mix to yield a zero net coupling factor. Multiple types of migration mechanisms have been reported in MD simulations including zig-zag motion (22), mixed rigid sliding/coupled motion (43), and mixtures of disconnection nuclei in the plane of the GB (44). These observations underscore the nonuniqueness and flexibility of GB migration mechanisms.

Many MD studies in bicrystals have reported apparent non-Arrhenius mobility behavior, including antithermal behavior in which mobility decreases with increasing temperature over some temperature interval (45–48). Several explanations for antithermal behavior have been proposed that may be true in different circumstances. These explanations include phonon-damped motion with very small energy barriers in the case of faceted twin GB motion (16, 45) and temperature-dependent mixtures of disconnection modes for other GBs (27).

It is unlikely that most curved GBs can move via disconnection glide alone. Climb-mediated disconnection motion, heterogeneous disconnection nucleation, and dislocation annihilation reactions are important topics for understanding curved GB migration. Vacancies have been shown to reduce the line tension and nucleation barrier of disconnections in several symmetric tilt GBs (49). Immobile disconnections have also been shown to act as sources of disconnections with reduced nucleation barriers compared with those in flat GBs (50). Climb phenomena are typically considered out of the timescale of MD, but solute drag has recently been analyzed in the drag regime in MD simulations (51). This was shown to be possible because of rapid GB diffusion, which enables solute drag on short timescales. Disconnection motion in MD simulations has been observed to coexist with GB diffusion (40, 44), and the interplay between the two effects is poorly understood. Recent MD simulations by Wang et al. (52) found that GB migration in thin surface crystals of Au-Si was controlled by through-thickness diffusion of Au atoms from the abutting liquid layer, which allowed for nonconservative dislocation motion and ultimately elimination of all GBs in the thin film.

The well-known survey of GB mobility in FCC Ni (48) revealed anisotropic mobilities spanning several orders of magnitude. The anisotropic distributions of these mobility values at fixed misorientation do not compare well to experimental GB velocity distributions (17). Although the comparison is not one-to-one (two different quantities are compared across very different length scales), the experiments call into question whether atomistic bicrystal migration simulations can give insight into anisotropic mobilities observed in polycrystalline materials. We believe that more detailed MD studies specifically targeted toward interesting experimental results are needed in nanocrystalline systems (as opposed to bicrystals), including studies of disconnection-mediated TJ migration along the lines of references (22, 53) and measurement of velocity distributions of individual GBs.

Little is still known about the detailed dynamics of atomic rearrangement during GB migration at realistic temperatures, as noted in Section 2.3 on HRTEM observations. A schematic of GB migration mechanisms (**Figure 3**) as described by Cahn et al. (40) illustrates that disconnection motion involves the shuffling of atoms in addition to shear displacement. A recent systematic

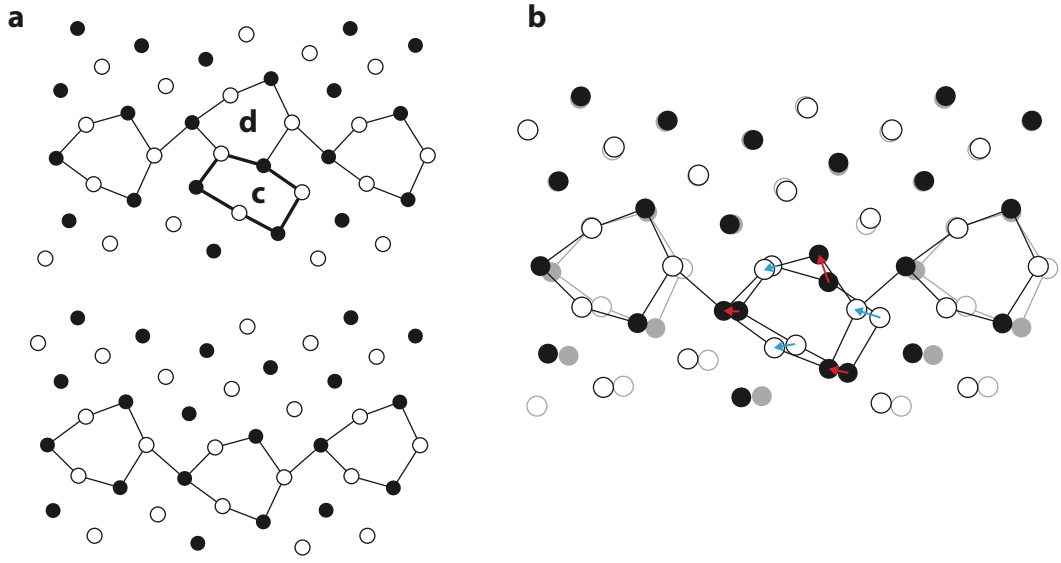

Figure 3

Migration mechanism of the Σ17(530)[100] 61.9° symmetric tilt grain boundary (GB) in face-centered cubic Cu as reported at room temperature under a strain-controlled driving force in the work of Cahn et al. (40). The initial and final states of the GB separating a disconnection nucleation event are shown in panel *a*. Atoms are colored by the (200) plane into the page, and two structural units are labeled c and d such that c transforms to d during migration. In panel *b*, initial and final states are superimposed and the displacement field between structural units c and d is shown. The shuffling character of motion is apparent from atomic displacements normal to the GB plane (top two displacements), and the shear character of motion can be seen from the horizontal leftward displacements of the bottom crystal (bottom four displacements).

survey of shuffling patterns during GB migration (44, 54) demonstrates that at intermediate temperatures (0.8 T_m or smaller), low-Σ GBs often exhibit highly ordered shuffling patterns that are distance minimizing in the dichromatic pattern. Furthermore, small translations at the GB chosen on the basis of minimum GB energy in MD simulations were found to significantly impact shuffling patterns of low-Σ GBs (44), highlighting the sensitive dependence of mobility anisotropy on translational microscopic degrees of freedom. Multiple shuffling patterns were found to compete for the same nominal disconnection mode during twist GB migration, and diffusion was always prevalent in the migration of general high-Σ GBs. Previous MD work (55) has shown that GB migration is a type of dynamical heterogeneity in which clusters of mobile atoms form and dissolve in a collective manner. Statistical tools and experimental methods (56) from the study of dynamical heterogeneity in glasses and liquids are anticipated to be useful in the study of GB migration, especially in strongly disordered GBs.

2.3. Microscopic Observations of Grain Boundary Migration

In situ TEM is a beneficial tool for directly observing GB motion. Observations of atomic shuffling and ledge-type movement have been used to support or contradict proposed GB motion mechanisms. However, the interpretation of these images and videos is not straightforward. TEM images are intrinsically 2D projections of a 3D specimen of finite thickness. Therefore, atomic motion (or lack thereof) above and below the focal plane can be lost or convolute the image.

The inability to account for the atomic structure along the entire 2D boundary has led the community to focus on particular GB types that may or may not be representative of general GB

motion in polycrystals. Most studies focus on high-symmetry GBs in thin films (53, 57, 58) or bicrystals (59–62). GBs in textured thin films have the advantage that neighboring grains have a common zone axis aligned so that atomic columns can be viewed simultaneously on both sides of the boundary. Additionally, columnar grains in films present GBs in the edge-on condition (i.e., incident electron beam parallel to the GB plane), revealing more information about the atomic positions.

The morphology of these GBs and the nature of the technique also restrict practical driving forces for GB motion. While GB migration during grain-growth studies is driven by the GB excess energy, bicrystal experiments using TEM require external driving forces (such as stress) for motion. Stress has been applied mechanically (60, 62, 63), through a preprocessed crack (64), or by the electron beam itself (61). In some studies, the driving force is not controlled but rather the result of different surface energies of the grains in thin samples (58) or due to interactions with the electron beam–induced defects (59). Despite these challenges, TEM studies of GB migration often show exciting results.

Discontinuous GB motion is often observed in in situ TEM studies. GBs jump (53, 58, 62), reverse direction (57, 58, 62), bulge (57), restructure (61), and oscillate between positions (64, 65). Often these movements are attributed to triggering events (58) that involve other vicinal defects such as stacking faults (59), twins (58), TJs (53, 62), and free surfaces (53, 62, 65). These behaviors have been used to support both cooperative shuffling and disconnection-mediated mechanisms, as discussed in Section 2.2.

Merkle et al. (58) observed GB migration in thin films of Au and Al with HRTEM. Most GBs moved through a series of jumps and stops, consistent with previous observations by Babcock & Balluffi (57) in Ag. The jumps occur near defects such as stacking faults or local distortions at TJs. One particular GB moved 2 nm within 0.07 s. A snapshot taken during this transition shows a moiré-like pattern within the distance traversed by the boundary, indicative of a cooperative shuffle of many atomic columns (see **Figure 4*a–d***). Such cooperative shuffles suggest that the GB migrates via a series of structural transitions.

Distinct structural transitions were observed by Wei et al. (61) in a $\Sigma 7(2\bar{3}10)/[0001]$ GB in alumina. The GB motion comprises a series of small coordinated atomic translations such that the boundary transitions between three different GB structures. In corresponding MD simulations, all three structures were found to be of low energy, indicating a low energy cost to transition between states. It is important to note that strain induced by the electron beam was used to drive GB motion in this study. The electron beam introduces strain by imposing point defects, which may segregate to the boundary and contribute to the motion mechanism.

Bowers et al. (59) observe that a cooperative atomic shuffle led to ledge-type motion in Au. Specifically, they observe the advance of a ledge via a jump several atomic planes wide due to interactions with the electron beam. The jump is achieved by cooperative atomic shuffling that allows both the ledge and an associated stacking fault to coalesce with another step along the boundary. The authors assert that the initial ledge is pinned by the stacking fault and that shuffling is the necessary pathway for motion to continue. They support this assertion by tracking the GB energy during the transition with a MD simulation. They find that the energy barrier for the boundary to move between states is similar to that needed to constrict the stacking fault.

In addition to these shuffling observations, several studies have showed a step-type growth ascribed to disconnection-mediated motion (53, 62, 65). Specifically, these observations show a step propagating parallel to the boundary, allowing the boundary to move forward without changing its atomic structure. Subsequent motion occurs from disconnection nucleation at TJs or free surfaces. Zhu et al. (62) observed this motion in a $\Sigma 11(113)$ GB in Au when a mechanical shear stress was used to drive GB migration. MD simulations find that it is energetically favorable for the

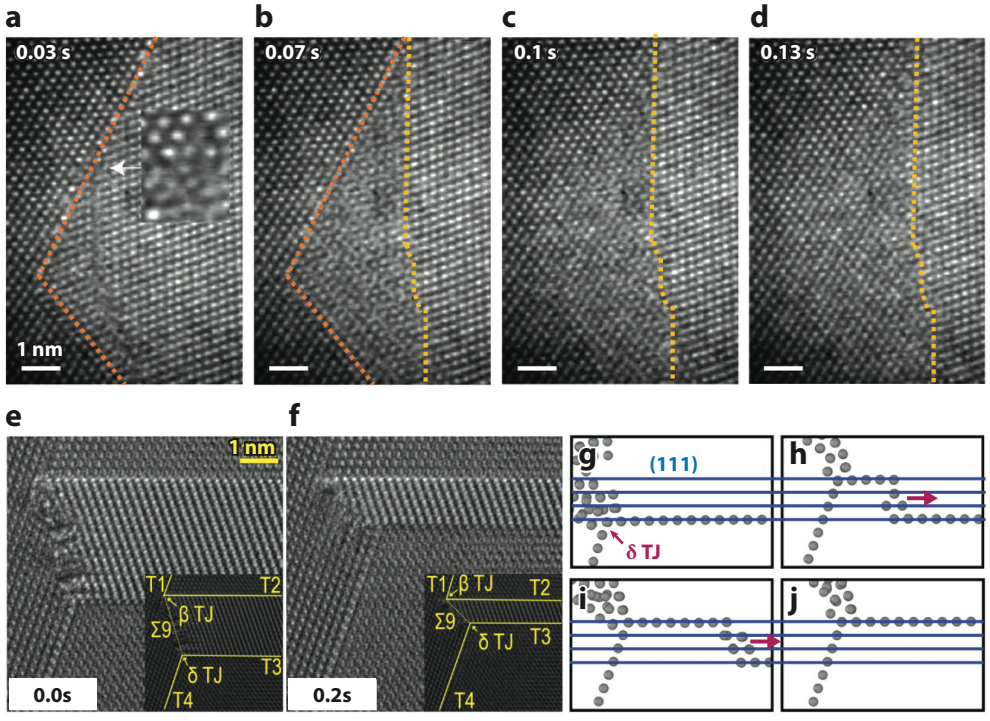

Figure 4

In situ high-resolution transmission electron microscopy observations supporting (*a–d*) a cooperative shuffling mechanism and (*e–j*) disconnection-mediated grain boundary (GB) motion. (*a–d*) Video frames of a Σ9 Au boundary moving at 823 K. Orange and yellow dashed lines were added to indicate the initial and final GB position, respectively. Panels *a–d* reproduced from Merkle et al. (58) with permission from Springer Nature. (*e–f*) Select video frames showing twin annihilation by GB motion in Cu. The disconnection-based migration mechanism was supported by molecular dynamics simulations, as shown in panels *g–j*, where the disconnection was nucleated at a triple junction (TJ). Individual twin boundaries are labeled T1, T2, T3, and T4. The images show one migrating TJ (β) and one stationary TJ (δ). Panels *e–j* reproduced from Xu et al. (53) (CC BY 4.0).

steps to coalesce; this coalescence appears as large jumps in the GB position. Zhu et al. (62) also showed that the step-type motion is unaffected by stacking faults and is prevalent in other tilt GBs, suggesting it is a general phenomenon.

In situ TEM studies also indicate that GB migration is sensitive to boundary crystallography. Unique motion mechanisms are attributed to GBs of different atomic structure (60, 65), misorientation (53, 58, 63, 64), and energy (53, 65). Furthermore, Merkle et al. (58) observed a transition in GB motion when a boundary changed inclination: A relatively immobile boundary comprising steps changed inclination and restructured as it traversed through a twin. After restructuring, the now-flat boundary jumped greater distances at a higher frequency, resulting in a greater velocity than the original GB structure had. This is consistent with recent observations of GB inclination–dependent GB velocities (17), described in Section 3.3.2.

GB energy plays a complicated role in the motion mechanism because it influences the atomic structure and the driving force itself. One example of this is in $SrTiO_3$, when the GB energy anisotropy leads to GBs dominated by (100) and (110) facets (66, 67). In this case Sternlicht et al. (65) concluded that GB migration was dominated by a ledge-type growth mechanism on these two facets. GB energy was also important in the results reported by Xu et al. (53), who studied a TJ in Cu comprising two low-energy twins and a higher-energy Σ9 boundary (see **Figure 4*e–f***). One

twin makes a series of jumps that span several atomic planes at a time, which allows the Σ9 boundary to shorten, reconfigure, and eventually disappear. The camera is not fast enough to capture the transition states of the boundary during the jump. Instead, the authors use MD simulations to support disconnection-mediated motion. Additionally, they use the MD simulations to demonstrate that the observed motion is not predicted when using shear as a driving force. Their observations suggest that the difference in energy of adjacent boundaries is responsible for the local motion.

3. GRAIN BOUNDARY MIGRATION AT THE CONTINUUM SCALE

3.1. The Driving Force for Grain Boundary Migration

Grain boundaries migrate to reduce the excess interfacial energy, and, assuming the energy change is path independent, the energy dissipated is equal to the driving force. The driving force for the oversimplified case where all GBs are assumed to have the same energy is considered first. The driving force for the realistic case where different GBs have different energies is considered next, and the driving force for the migration of singular GBs is considered in the final subsection.

3.1.1. The migration of grain boundaries with uniform energies. Historical research on GB migration has typically been carried out under the assumption of uniform GB properties. For this reason, soap froths, whose cell boundaries have uniform curvature and isotropic energies, were often taken as analog models for polycrystals before computer simulations were possible (68, 69). Ignoring for the moment that the assumption of uniform GB energy for crystals is incorrect, the soap froth analogy fails in two other important ways. First, within a bubble in a soap froth, pressure is uniform at all points. Because atoms are not able to freely move large distances in a crystal (as compared with atoms in a gas), there is no expectation of uniform pressure on a boundary (70). Second, the evolution of a soap froth is driven by pressure differences between the bubbles; gas atoms diffuse through the cell walls from one bubble to another (68). Compared with the driving force provided by the surface energy, the driving force provided by the pressure difference between grains in a polycrystal is negligible (7, 71). The pressure (P) equals $2\gamma/r$, and the elastic energy per volume is therefore P^2/E, where E is the elastic modulus. This means the elastic energy of a spherical grain of radius r is $4\pi r^3 P^2/3E$. Comparing that to the GB energy of the spherical grain ($4\pi r^2\gamma$), the ratio of the elastic and GB energies (ε) is

$$\varepsilon = \frac{4\gamma}{3Er}. \qquad 4.$$

If we take γ to be ¾ J/m^2 and E to be a typical value of 100 GPa, then $\varepsilon = 10^{-11}$ m/r. According to this reasoning, the elastic energy of a 1-nm crystal is only 1% of the GB energy and is progressively less for larger crystals. Therefore, pressure is irrelevant to the driving force for GB migration, and this oft-used term should be avoided. It is the excess GB energy that provides the driving force for GB migration.

The classical isotropic model of GB migration, described in Section 2.1.1, forms the basis for our current understanding of the topic. The idea that GBs migrate, according to Equation 1, toward their centers of curvature also leads to topological rules for GB migration in two (70) and three (72) dimensions. Recent 3D experimental observations, as described in Section 3.3.2, provide limited support for topological theories of grain growth (73–76). Nevertheless, the relationship between the change in mean grain size with time (a proxy for GB velocity) and the inverse mean grain size (a proxy for curvature) usually agrees with the proposed linear relationship between velocity and curvature and is often used to compute average GB mobilities (77).

3.1.2. The migration of grain boundaries with anisotropic energies. While the assumption of uniform GB properties simplifies the definition of the driving force for migration, it is an oversimplification. Recent experimental observations point to the fact that simple ideas based on curvature and topology do not explain the changes in volumes of individual grains (73, 75, 76), and others question the validity of the simple linear relation between curvature and velocity (17–19). GB energy anisotropy is one feature that is almost certain to be important. Ignoring the microscopic degrees of freedom, there are five macroscopic parameters that must be specified to differentiate one GB from another. For example, the lattice misorientation is described by three parameters, and the orientation of the GB plane is described by two parameters. While the assumption of isotropic GB properties might have been necessary 20 years ago, since then we have learned a great deal about the variations in GB energy as a function of the five bicrystal parameters from experiments (78–81) and simulations (82, 83). There are even functions that interpolate the existing data that make it possible to approximate the energy of any boundary for some FCC and body-centered cubic materials (84, 85). With this information available, one can compute the driving force for the migration of grain boundaries with anisotropic energies as specified by Herring (71). At point i on the boundary, the velocity is

$$v_i = M_i \left[\left(\gamma_i + \frac{\partial^2 \gamma_i}{\partial \theta_1^2} \right) \kappa_1 + \left(\gamma_i + \frac{\partial^2 \gamma_i}{\partial \theta_2^2} \right) \kappa_2 \right], \qquad 5.$$

where Equation 5 applies to each point of interest where γ_i is the GB energy at that point, M_i is the GB mobility, and κ_1 and κ_2 are the principal curvatures. The derivatives with respect to θ_1 and θ_2 measure the changes in surface energy with respect to changes in the orientation of the surface normal in the two principal directions. The terms in parentheses are referred to as the GB stiffness. These terms can now be determined by analysis of GB energy functions fit to discrete data (86, 87) or computed by simulations (88). It should be emphasized that experimentally measured GB energies and computed energies agree that there is more anisotropy in the GB plane orientation than in misorientation (10). As a result, the second derivatives of the energy can be as large or larger than the energy itself. This means that the stiffness terms in Equation 5 can have a significant effect on the velocity, which is not predicted by Equation 1. A feasible near-term challenge is to compare measured migration velocities to computed stiffnesses to see if they obey Equation 5.

3.1.3. The migration of a singular grain boundary. A singular GB occurs at the orientation of a cusp in the energy as a function of GB plane orientation. Such boundaries are flat and have a curvature of exactly zero, so Equations 1 and 5 predict that they will not migrate. While they might not be numerous in all polycrystals, the existence of some singular boundaries is a certainty (for example, the coherent twin in FCC materials). The role of singular GBs in microstructure evolution has been debated (21), and they remain poorly understood. Herring (71) recognized that the migration of a singular boundary was a special case and had to be considered separately. With reference to **Figure 5**, we consider a section plane through a singular boundary attached to four other boundaries at triple lines. Assume the upper boundaries have energies γ_1, the singular boundary has energy γ_0, and the lower boundaries have energy γ_2, such that $\gamma_0 < \gamma_1 < \gamma_2$. If we assume there is no barrier to nucleating new layers of atoms on the singular boundary and imagine it moves an incremental distance δ while preserving the dihedral angles, then the energy change is $\delta\gamma_0 \sin\alpha + \delta\gamma_1 \sin\beta - \delta\gamma 2 \cos\alpha$. This motion decreases the energy as long as $\gamma_2 > \gamma_0 \tan\alpha + \gamma_1 \sin\beta/\cos\alpha$. In other words, the driving force is supplied by eliminating higher-energy boundaries and replacing them with lower-energy boundaries, without the need for curvature. Migration of this type has been observed for the growth of corner twins (89). While this provides the driving force for the migration of singular boundaries, the same driving force must also occur during the migration of anisotropic nonsingular boundaries. For example, **Figure 5*c*** illustrates

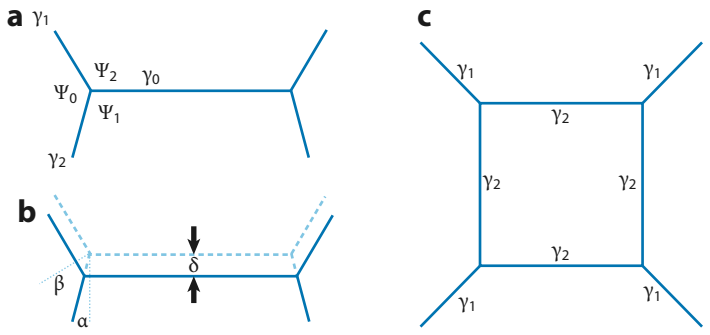

Figure 5

The migration of a singular boundary. (*a*) Grain boundaries (GBs) with energies γ_1 and γ_2 meet a singular boundary with energy γ_0. (*b*) The GB after migrating a small distance, δ. The dashed lines show the original boundary positions, and α and β define the angles used to compute the energy change that results from migration. (*c*) A square grain, with GB energies of γ_2 with the surrounding grains. Where the surrounding grains meet, the GB energies are γ_1.

a four-sided grain, which should shrink if all GB energies are equal. However, in the case that $\gamma_1/\gamma_2 > \sqrt{2}$, the four-sided grain will grow, replacing the higher-energy GBs with energy γ_1 with lower-energy GBs with energy γ_2. The driving force depends in a sensitive way on the exact boundary energy anisotropy and interfacial geometry. The driving force under these conditions has been generalized using the concept of weighted mean curvature (90). This is an unfortunate choice of terminology, because the migrating interface has zero curvature.

3.2. Simulations of Grain Boundary Migration During Grain Growth

Simulations of GB migration at the continuum level have been demonstrated with the Monte Carlo method (91), MD (21, 92), phase-field methods (93, 94), and other approaches. Here, we focus on simulations based on the threshold dynamics (TD) model; this is an extension of the mean curvature approach (95, 96) to a general setting with multiple grains (97). TD provides an efficient numerical approximation scheme for migration driven solely by capillarity. Further, it can be enhanced to account for GB energies that depend on the lattice misorientation and the GB normal (five parameter–dependent GB energies). Compared with alternative methods such as phase-field modeling (98), TD does not need as fine a mesh to resolve the interfaces, thereby permitting much larger simulations that make it possible to perform grain evolution calculations over the entire experimentally sampled volume. On the other hand, phase-field modeling can readily couple to the stress through momentum balance (99–101), which is not possible with current formulations of TD.

3.2.1. Simulations assuming uniform boundary properties. Peng et al. (102) used TD (97) to compare, in a grain-by-grain fashion, simulations and experimental observations of grain growth at several annealing stages. The detailed nature of the comparison provided insights into the differences between the predictions of this model and experiments. The method reproduces the expected growth kinetics. However, a significant discrepancy was found for the smallest grains; the isotropic TD simulation predicted that these grains would shrink and disappear at greater rates than were observed in the experiment. This error then propagated to the predictions for the number of neighbors for each grain. In particular, the largest errors in the predicted volume changes were associated with the grains whose number of neighbors was predicted incorrectly.

Better predictions might be expected if one accounts for anisotropic GB properties. However, because the discrepancy is greatest for the smallest grains, it is possible that unidentified size effects might also be important. The problem of accurately simulating observed grain size distributions has been discussed by Barmak et al. (103), and the few instances where simulations were directly compared with experimental data also concluded that the simulations do not accurately reproduce the experiments (9, 102, 104).

3.2.2. Simulations with anisotropic grain boundary properties. Grain growth under the assumption of anisotropic GB properties has been simulated by a variety of methods (20, 94, 105–107). Using a 2D grain-growth simulation model with fully anisotropic GB properties, Florez et al. (20) showed that when anisotropic GB energies are assumed, some GBs move opposite to the direction predicted by their curvature, as observed in recent experiments and in defiance of Equation 1 (17, 18). TD is also compatible with anisotropic energies and mobilities (108) that are obtained from experimental observations (10, 17). However, there are a number of practical challenges that must be addressed. A key challenge is that the experimental volume contains a large number of different GB types because the parameter space is five-dimensional. While the energies are available from existing data (10, 84, 85), dealing with this directly is prohibitively expensive numerically. Specifically, it is necessary to compute a different convolution kernel—the key step in TD—for every grain pair.

Tools from data science can be used to address this challenge (109, 110). First, standard regression techniques are used to approximate the experimental data for the GB energy using a closed-form function. The GB energy data are provided discretely for 36 points with different azimuthal and polar angles of the GB normal on the unit sphere. These are converted from the spherical representation to Cartesian representation, fit to the data using kernels that are directional Gaussians, and used to compute the associated anisotropic kernels. Next, to deal with the extremely large number of grain pairs, a hierarchical agglomerative clustering algorithm is used to group grains with low misorientation with respect to each other to decrease the number of distinguished boundaries. This makes it possible to compute only those kernels that are not repeated, reducing the computational time by one-to-two orders of magnitude.

A sensitive test of such a simulation is to compare the simulated and observed GB plane distribution, as this is a structural characteristic closely linked to the GB energy anisotropy (111). The GB plane distribution for the $\Sigma 3$ GB of Ni has a peak at the (111) twin position of 390 multiples of a random distribution (MRD) in the data used as a starting point for the simulation. When the evolution of this microstructure is simulated with isotropic energies, the relative area of the twin declines to 250 MRD after a small increase in grain size (see **Figure 6*a***). In other words, the simulation makes the structure more isotropic. However, when anisotropic energies are assumed with a minimum at the twin position (see **Figure 6*b***), the relative area of the twin is maintained at approximately 360 MRD, similar to that found in the initial structure.

3.3. Experimental Observations of Grain Boundary Migration

Grain boundary migration has been observed in specimens containing only a single boundary (bicrystals) and in those containing many boundaries (polycrystals). The main difference between these cases is that the motion of a GB in a bicrystal is unconstrained by any other boundaries while in the polycrystal, the motion of any boundary affects the areas of all attached GBs.

3.3.1. Bicrystals. Bicrystal experiments have been used to demonstrate that GB migration depends on driving force, misorientation, and plane inclination, in agreement with Equations 1 and 2 (13, 112–114). The bicrystal geometry controls the driving force for accurate measurements of

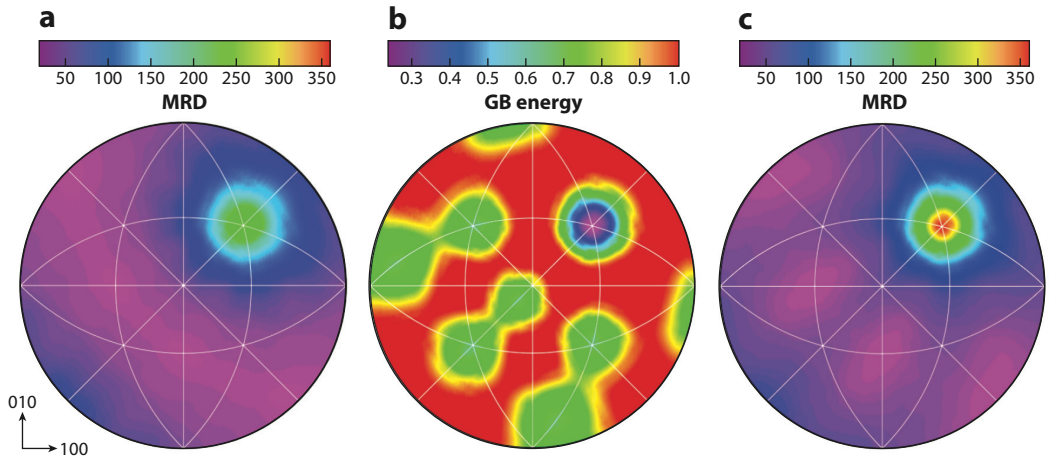

Figure 6

Stereographic projections of (*a*,*c*) GB plane distributions and (*b*) GB energy at the Σ3 misorientation. (*a*) The GB plane distribution after evolution, assuming isotropic GB energy. (*c*) The GB plane distribution after evolution, assuming the anisotropic GB energies shown in panel *b*. Abbreviations: GB, grain boundary; MRD, multiples of a random distribution.

properties including activation energy and reduced mobility, which are otherwise unattainable in traditional grain-growth studies. Sun & Bauer (115) introduced a wedge-type geometry in which the boundary meets the sample surface at a sharp angle and the curvature decreases with migration. The half-loop and quarter-loop geometries maintain a constant curvature as the GB migrates (24, 92). Bicrystals with a uniform plane inclination can also be used but require an external driving force such as an applied shear stress (114) or magnetic field (116) to induce migration. These studies, regardless of geometry, find that the activation energy and, thus, the mechanism for motion are dependent on misorientation and plane inclination in metals with cubic (92, 117, 118) and hexagonal (116) crystal structures and in ceramics (115).

A magnetic field driving force was used to evaluate the effect of anisotropic GB energy on GB migration in a bicrystal (119). The special geometry included notches on the sample surface that pinned the boundary and prevented it from moving freely. The magnetic field drives the crystal of preferred orientation to grow, causing the pinned GB to bend and lengthen until it reaches an energy balance between the capillary and magnetic driving forces. The boundary should have uniform curvature when GB energy is independent of plane inclination. However, a symmetrical 90° <112> Bi boundary evolved into three macroscopic facets defined by different plane inclinations of low energy. Furthermore, ledges associated with these facets prohibited the boundary's motion such that it had not yet reached its equilibrium length. Although driven by a magnetic field, this observation indicates GB restructuring is favorable and influences the migration behavior. Despite the influence of anisotropic energies in this case, the vast majority of bicrystal experiments indicated that GBs migrate in a way consistent with Equation 1, with a mobility that varies with the GB crystallography.

3.3.2. Grain boundary migration in polycrystals. As noted in Section 1, HEDM (8) and DCT (9) have recently made it possible to monitor the changes in the shape and size of many grains in an opaque polycrystalline material as a result of thermal annealing. While the methods are currently limited to a resolution of a few micrometers, choosing the appropriate grain size and annealing interval make it possible to monitor GB migration at this length scale. To date, a small number

of grain-growth (9, 73, 75, 120, 121) and coarsening (122) studies have been reported that have provided numerous insights, including those that challenge accepted models of grain growth based on curvature and topology.

The first nondestructive study of grain growth was directed at β-Ti, the structure of which was studied by edge-enhanced X-ray tomography (9). While the material was single-phase at the temperature where grain growth occurs, α-Ti precipitates on the GBs during cooling, and this makes it possible to determine the boundary positions by tomography. Unfortunately, this technique does not provide information about the grain orientations. The experiment was simulated using a phase-field model that assumed uniform GB properties. The phase-field simulation provided excellent agreement in some areas, presumed to have isotropic GB energies, and poor agreement in others, where the observed grain shapes were not reproduced. It was proposed that the poor agreement occurs in situations where there were anisotropic GB properties.

Five 3D, nondestructive grain-growth studies have been conducted that compare grain characteristics such as size, number of near neighbors, integral mean curvature, and mean width to the volume changes of grains in Ni (73), $SrTiO_3$ (120), and α-Fe (75, 76, 121). From these studies, one can conclude that while the averages of these grain characteristics correlate to average grain volume changes, consistent with isotropic models of microstructure evolution, individual grains deviate by large amounts from this simplified model, and this deviation was greatest in the most anisotropic materials [Ni (73) and $SrTiO_3$ (120)]. For example, in Ni, correlation between a grain's volume change and its geometric and topological characteristics was detected only after adjacent twin-related domains were merged into single grains. Furthermore, even with this simplification, the best predictor for the sign of the volume change was correct only 65% of the time (73).

There have been several recent experimental attempts to consider the effect of GB crystallography on GB migration, and all have provided surprising information (17, 19, 123). For example, measurements of a cube-textured Al-1 wt% Mg alloy indicated that for any particular misorientation angle, the dispersion of velocities was much larger than variations of the mean value as a function of misorientation (123). A phase-field simulation has been used to model observed grain growth in α-Fe (19). The observations included 1,501 grains, and the simulation was constructed under the assumption that Equation 1 is correct, meaning that a mobility-energy product was determined from the experimentally observed velocity and curvature. The surprising result was that the mobilities of 1,619 grain boundaries determined in this way were uncorrelated to the boundary crystallography and, for the same boundary, were not constant with time. More specifically, GBs with nearly identical crystallographic parameters had mobilities that differed by as much as a factor of nine. This observation draws into question any relationship between GB mobility and GB crystallography (as observed in bicrystals). However, we should also recall that several of the experiments described above (73, 75, 76) cast doubt on the role of curvature on GB migration in polycrystals, so we must also consider the possibility that the assumed linear relation between velocity and curvature (Equation 1) is not correct.

Measurements of GB velocities in polycrystalline Ni concluded that GB velocity was not correlated to curvature (17). In this study, the velocities of more than 5×10^4 boundaries were compared with their curvatures. The results, illustrated in **Figure 7**, show that velocity and curvature are uncorrelated. More recently, similar data for $SrTiO_3$ supported the same conclusion (18). The images in **Figure 8** illustrate individual boundaries that did not evolve in accordance with Equation 1. In **Figure 8*a***, a flat boundary with zero curvature migrates during annealing, and in **Figure 8*b***, a boundary migrates away from its center of curvature.

When the observed velocities for Ni are classified according to all five parameters that characterize the bicrystal, systematic trends are revealed, as illustrated in **Figure 9**. The velocities of all GBs with the Σ3 misorientation (60°/[111]) are illustrated in **Figure 9*a*** as a function of

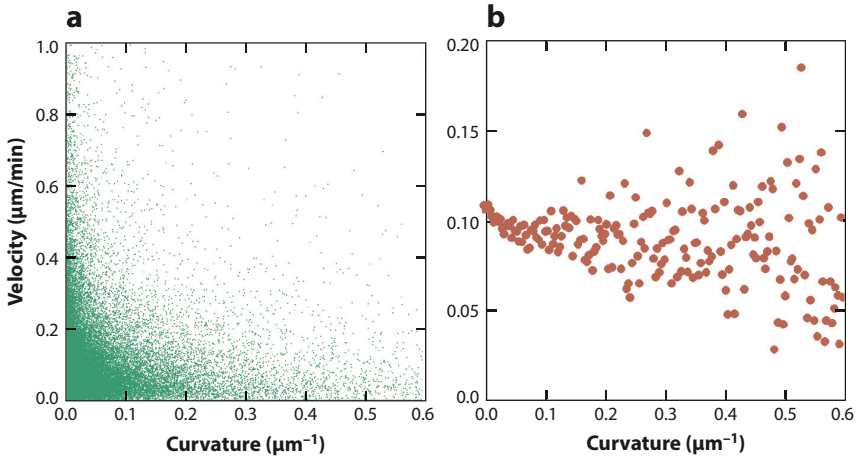

Figure 7

The grain boundary velocity as a function of curvature. (*a*) Scatterplot showing the entire domain of the data. (*b*) Mean velocities of boundaries classified into curvature groups with widths of 0.003 μm^{-1} (17).

GB plane orientation. One can see that the minimum velocity occurs for the (111) coherent twin boundary and boundary planes perpendicular to this orientation have higher velocities. When compared with the curvatures (**Figure 8*b***), the twin boundary is also a minimum, as expected for a singular boundary. However, the orientations of maximum velocity do not correlate with the

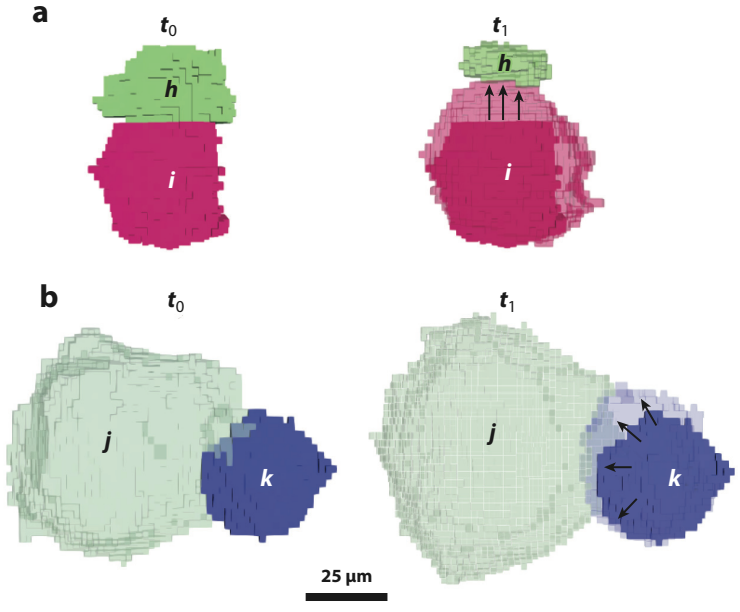

Figure 8

Evolution of two grains during annealing. (*a*) In the initial state (t_0), the grain boundary between *h* and *i* is flat, with zero curvature. The final state (t_1) shows that the boundary between *h* and *i* did not have zero velocity. (*b*) The boundary between *k* and *j* migrates away from its center of curvature during annealing. Figure adapted with permission from Reference 18.

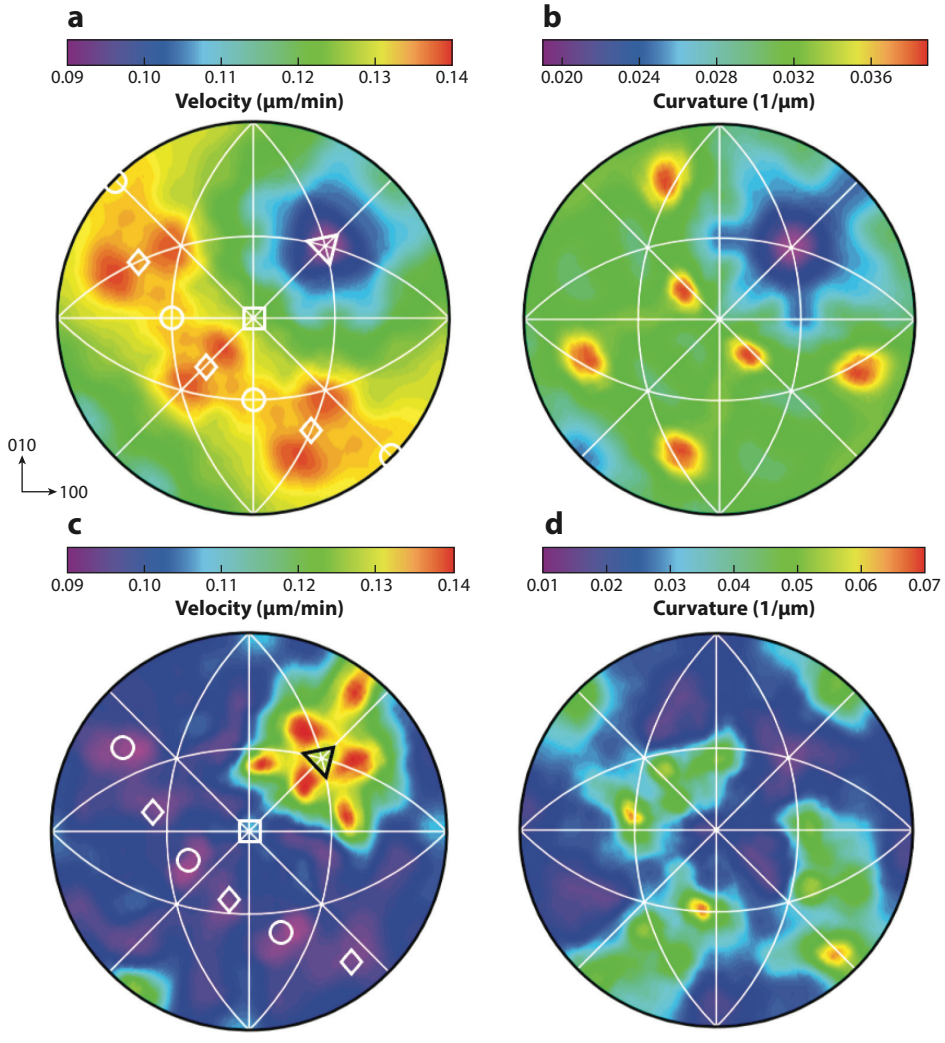

Figure 9

Velocities and curvatures of (*a*,*b*) Σ3 and (*c*,*d*) Σ7 grain boundaries (GBs) in Ni plotted on stereographic projections along [001], with the velocity (*a*,*c*) in μm/min and the curvature (*b*,*d*) in 1/μm. In panels *a* and *c*, the [001] direction is at the position of the white square, and the [111] misorientation axis is at the position of the triangle. In panel *a*, the white circles and diamonds mark the orientations of tilt GBs with $\{\bar{1}10\}$ and $\{\bar{2}11\}$ GB planes, respectively. In panel *c*, the white circles and diamonds mark the orientations of tilt GBs with $\{\bar{3}21\}$ and $\{\bar{5}14\}$ GB planes, respectively (17).

maximum curvature. The absence of a positive correlation is also evident in the data for the Σ7 grain boundaries (38°/[111]), which suggests that the velocity and curvature are anticorrelated for this misorientation (**Figure 9*c*,*d***). These data indicated that unlike in bicrystals, in polycrystals curvature is not the decisive factor that determines the direction or speed of GB migration.

When measurements of GB migration in bicrystals (Section 3.3.1) and polycrystals are compared, both agree that migration velocities depend on the GB degrees of freedom. However, while the bicrystal results are consistent with Equation 1, the results from polycrystals are not. In bicrystals, GBs move without constraint under an easily quantified driving force. In polycrystals,

a boundary cannot move without the concerted motion of all connected GBs, and the driving force depends not only on the change in that area and the energy of the boundary of interest but also on the changes to the attached boundaries (as illustrated in **Figure 5**).

4. SUMMARY OF CURRENT KNOWLEDGE AND FUTURE DIRECTIONS

The status of current knowledge about GB migration in polycrystals, which has recently advanced by the development of X-ray microscopy techniques and theories for defect-mediated migration, suggests that significant discoveries remain to be made. We conclude this review with three overarching assertions that are supported by a consensus of recent research together with some suggested paths for continued research.

- GB migration rates depend on the five parameters that characterize the bicrystal geometry. This assertion is supported by experiment, theory, and simulation. However, the mechanism that links structure to migration velocity is currently unclear, and it is not obvious if the same GB migration velocity–structure relationships observed for bicrystals govern the migration of GBs in polycrystals. A clear path for research would be to rigorously compare migration velocities predicted by the defect-mediated migration theory for a wide selection of boundary types, spanning boundaries from the minimum to the maximum expected velocities, to experimental observations and to MD simulations of GB motion in polycrystals.
- The simple linear relation between GB velocity and curvature found in bicrystals is inconsistent with the migration of GBs in polycrystals. It seems clear that the true driving force for GB motion is more complex than simply reducing the radius of curvature of a single GB. Because different boundaries have different energies, and a single boundary cannot move without changing the areas of other boundaries, the driving force for migration must include the changes in the energies of all of these boundaries. With the recent ability to specify the GB energies as a function of all five parameters for many materials, it should be possible to quantify this driving force and compare it to experimentally observed motion. Similarly, knowledge of these energies now makes it possible to consider the influence of GB stiffnesses (Equation 5) on the velocity.
- Simulations of microstructure evolution that assume uniform GB properties do not make accurate predictions of how real materials evolve. The availability of 3D observations of real materials provides a standard against which the simulations can be compared. The obvious step in this area is to add appropriate descriptions of the anisotropic GB properties to the microstructure evolution model, although challenges to this task remain.

DISCLOSURE STATEMENT

The authors are not aware of any affiliations, memberships, funding, or financial holdings that might be perceived as affecting the objectivity of this review.

ACKNOWLEDGMENTS

This work was supported by the National Science Foundation under Designing Materials to Revolutionize and Engineer our Future (DMREF) grant 2118945.

LITERATURE CITED

1. Kang S-JL, Park J-H, Ko S-Y, Lee H-Y. 2015. Solid-state conversion of single crystals: the principle and the state-of-the-art. *J. Am. Ceram. Soc.* 98:347–60

2. Perrin AE, Schuh CA. 2021. Stabilized nanocrystalline alloys: the intersection of grain boundary segregation with processing science. *Annu. Rev. Mater. Res.* 51:241–68
3. Gleiter H. 1969. Theory of grain boundary migration rate. *Acta Metall.* 17:853–62
4. Gottstein G, Molodov DA, Shvindlerman LS. 1998. Grain boundary migration in metals: recent developments. *Interface Sci.* 6:7–22
5. Smith DA. 1991. *On the mechanisms of grain-boundary migration*. Paper presented at the 1st International Conference on Grain Growth in Polycrystalline Materials, Rome, Italy
6. Turnbull D. 1951. Theory of grain boundary migration rates. *Trans. Am. Inst. Min. Metall. Eng.* 191:661–65
7. Gottstein G, Shvindlerman LS. 2010. *Grain Boundary Migration in Metals*. Boca Raton: CRC Press
8. Bernier JV, Suter RM, Rollett AD, Almer JD. 2020. High-energy X-ray diffraction microscopy in materials science. *Annu. Rev. Mater. Res.* 50:395–436
9. McKenna IM, Poulsen SO, Lauridsen EM, Ludwig W, Voorhees PW. 2014. Grain growth in four dimensions: a comparison between simulation and experiment. *Acta Mater.* 78:125–34
10. Rohrer GS. 2011. Grain boundary energy anisotropy: a review. *J. Mater. Sci.* 46:5881–95
11. Han J, Thomas SL, Srolovitz DJ. 2018. Grain-boundary kinetics: a unified approach. *Prog. Mater. Sci.* 98:386–476
12. Beck PA. 1952. Interface migration in recrystallization. In *Metal Interfaces*, pp. 208–47. Cleveland, OH: Am. Soc. Metals
13. Gottstein G, Shvindlerman LS. 1992. On the true dependence of grain-boundary migration rate on driving force. *Scr. Metall. Mater.* 27:1521–26
14. Zhang K, Weertman JR, Eastman JA. 2005. Rapid stress-driven grain coarsening in nanocrystalline Cu at ambient and cryogenic temperatures. *Appl. Phys. Lett.* 87:061921
15. Rheinheimer W, Hoffmann MJ. 2015. Non-Arrhenius behavior of grain growth in strontium titanate: new evidence for a structural transition of grain boundaries. *Scr. Mater.* 101:68–71
16. Homer ER, Johnson OK, Britton D, Patterson JE, Sevy ET, Thompson GB. 2022. A classical equation that accounts for observations of non-Arrhenius and cryogenic grain boundary migration. *npj Comput. Mater.* 8:157
17. Bhattacharya A, Shen YF, Hefferan CM, Li SF, Lind J, et al. 2021. Grain boundary velocity and curvature are not correlated in Ni polycrystals. *Science* 374:189–93
18. Muralikrishnan V, Liu H, Yang L, Conry B, Marvel CJ, et al. 2023. Observations of unexpected grain boundary migration in $SrTiO_3$. *Scr. Mater.* 222:115055
19. Zhang J, Ludwig W, Zhang YB, Sorensen HHB, Rowenhorst DJ, et al. 2020. Grain boundary mobilities in polycrystals. *Acta Mater.* 191:211–20
20. Florez S, Alvarado K, Murgas B, Bozzolo N, Chatain D, et al. 2022. Statistical behaviour of interfaces subjected to curvature flow and torque effects applied to microstructural evolutions. *Acta Mater.* 222:117459
21. Holm EA, Foiles SM. 2010. How grain growth stops: a mechanism for grain-growth stagnation in pure materials. *Science* 328:1138–41
22. Thomas SL, Chen KT, Han J, Purohit PK, Srolovitz DJ. 2017. Reconciling grain growth and shear-coupled grain boundary migration. *Nat. Comm.* 8:1764
23. Gleiter H. 1969. Mechanism of grain boundary migration. *Acta Metall.* 17:565–73
24. Gottstein G, Molodov DA, Shvindlerman LS. 2010. Grain-boundary energy and mobility. In *ASM Handbook* Vol. 22B: *Metals Process Simulation*, ed. DU Furrer, SL Semiatin, pp. 67–91. Materials Park, OH: ASM Int.
25. Hirth JP, Balluffi RW. 1973. Grain-boundary dislocations and ledges. *Acta Metall.* 21:929–42
26. Hirth JP, Pond RC. 1996. Steps, dislocations and disconnections as interface defects relating to structure and phase transformations. *Acta Mater.* 44:4749–63
27. Chen K, Han J, Srolovitz DJ. 2020. On the temperature dependence of grain boundary mobility. *Acta Mater.* 194:412–21
28. Thomas SL, Wei CZ, Han J, Xiang Y, Srolovitz DJ. 2019. Disconnection description of triple-junction motion. *PNAS* 116:8756–65

29. Admal NC, Ahmed T, Martinez E, Po G. 2022. Interface dislocations and grain boundary disconnections using Smith normal bicrystallography. *Acta Mater*. 241:118340
30. Combe N, Mompiou F, Legros M. 2016. Disconnections kinks and competing modes in shear-coupled grain boundary migration. *Phys. Rev. B* 93:024109
31. Rajabzadeh A, Mompiou F, Legros M, Combe N. 2013. Elementary mechanisms of shear-coupled grain boundary migration. *Phys. Rev. Lett.* 110:265507
32. Chen KT, Han J, Pan XQ, Srolovitz DJ. 2020. The grain boundary mobility tensor. *PNAS* 117:4533–38
33. Chen KT, Han J, Thomas SL, Srolovitz DJ. 2019. Grain boundary shear coupling is not a grain boundary property. *Acta Mater*. 167:241–47
34. Trautt ZT, Mishin Y. 2012. Grain boundary migration and grain rotation studied by molecular dynamics. *Acta Mater*. 60:2407–24
35. Thomas SL, King AH, Srolovitz DJ. 2016. When twins collide: twin junctions in nanocrystalline nickel. *Acta Mater*. 113:301–10
36. Rabkin E, Srolovitz DJ. 2020. Grain growth stagnation in thin films due to shear-coupled grain boundary migration. *Scr. Mater.* 180:83–87
37. Holm EA, Rohrer GS, Foiles SM, Rollett AD, Miller HM, Olmsted DL. 2011. Validating computed grain boundary energies in fcc metals using the grain boundary character distribution. *Acta Mater*. 59:5250–56
38. Rohrer GS, Holm EA, Rollett AD, Foiles SM, Li J, Olmsted DL. 2010. Comparing calculated and measured grain boundary energies in nickel. *Acta Mater*. 58:5063–69
39. Molodov KD, Molodov DA. 2018. Grain boundary mediated plasticity: on the evaluation of grain boundary migration - shear coupling. *Acta Mater*. 153:336–53
40. Cahn JW, Mishin Y, Suzuki A. 2006. Coupling grain boundary motion to shear deformation. *Acta Mater*. 54:4953–75
41. Taylor JE, Cahn JW. 2007. Shape accommodation of a rotating embedded crystal via a new variational formulation. *Interfaces Free Bound*. 9:493–512
42. Ren XB, Jin CH. 2020. Grain boundary motion in two-dimensional hexagonal boron nitride. *ACS Nano* 14:13512–23
43. Schratt AA, Mohles V. 2020. Efficient calculation of the ECO driving force for atomistic simulations of grain boundary motion. *Comp. Mater. Sci.* 182:109774
44. Chesser I, Runnels B, Holm E. 2022. A taxonomy of grain boundary migration mechanisms via displacement texture characterization. *Acta Mater*. 222:117425
45. Chesser I, Holm E. 2018. Understanding the anomalous thermal behavior of Σ3 grain boundaries in a variety of FCC metals. *Scr. Mater.* 157:19–23
46. Homer ER, Holm EA, Foiles SM, Olmsted DL. 2014. Trends in grain boundary mobility: survey of motion mechanisms. *JOM* 66:114–20
47. Humberson J, Holm EA. 2017. Anti-thermal mobility in the Σ3 [111] 60° {11 8 5} grain boundary in nickel: mechanism and computational considerations. *Scr. Mater.* 130:1–6
48. Olmsted DL, Holm EA, Foiles SM. 2009. Survey of computed grain boundary properties in face-centered cubic metals—II: grain boundary mobility. *Acta Mater*. 57:3704–13
49. Chen DK, Xu SZ, Kulkarni Y. 2020. Atomistic mechanism for vacancy-enhanced grain boundary migration. *Phys. Rev. Mater.* 4:033602
50. Combe N, Mompiou F, Legros M. 2019. Heterogeneous disconnection nucleation mechanisms during grain boundary migration. *Phys. Rev. Mater.* 3:060601
51. Koju RK, Mishin Y. 2020. Direct atomistic modeling of solute drag by moving grain boundaries. *Acta Mater*. 198:111–20
52. Wang MY, Peng Y, Wang HL, Upmanyu M. 2021. Coarsening of polycrystalline patterns in atomically thin surface crystals. *Appl. Phys. Lett.* 119:123102
53. Xu M, Chen K, Cao F, Estrada LV, Kaufman TM, et al. 2022. Disconnection-mediated twin/twin-junction migration in FCC metals. *Acta Mater*. 240:118339
54. Chesser I, Holm E, Runnels B. 2021. Optimal transportation of grain boundaries: a forward model for predicting migration mechanisms. *Acta Mater*. 210:116823

55. Zhang H, Srolovitz DJ, Douglas JF, Warren JA. 2006. Characterization of atomic motion governing grain boundary migration. *Phys. Rev. B* 74:115404
56. Berthier L, Biroli G. 2011. Theoretical perspective on the glass transition and amorphous materials. *Rev. Mod. Phys.* 83:587–645
57. Babcock SE, Balluffi RW. 1989. Grain-boundary kinetics—II. *In situ* observations of the role of grain boundary dislocations in high-angle boundary migration. *Acta Metall.* 37:2367–76
58. Merkle KL, Thompson LJ, Phillipp F. 2004. In-situ HREM studies of grain boundary migration. *Interface Sci.* 12:277–92
59. Bowers ML, Ophus C, Gautam A, Lancon F, Dahmen U. 2016. Step coalescence by collective motion at an incommensurate grain boundary. *Phys. Rev. Lett.* 116:106102
60. Rajabzadeh A, Legros M, Combe N, Mompiou F, Molodov DA. 2013. Evidence of grain boundary dislocation step motion associated to shear-coupled grain boundary migration. *Phil. Mag.* 93:1299–316
61. Wei JK, Feng B, Ishikawa R, Yokoi T, Matsunaga K, et al. 2021. Direct imaging of atomistic grain boundary migration. *Nat. Mater.* 20:951–55
62. Zhu Q, Cao G, Wang JW, Deng C, Li JX, et al. 2019. In situ atomistic observation of disconnection-mediated grain boundary migration. *Nat. Comm.* 10:156
63. Mompiou F, Caillard D, Legros M. 2009. Grain boundary shear–migration coupling—I. In situ TEM straining experiments in Al polycrystals. *Acta Mater.* 57:2198–209
64. Legros M, Gianola DS, Hemker KJ. 2008. In situ TEM observations of fast grain-boundary motion in stressed nanocrystalline aluminum films. *Acta Mater.* 56:3380–93
65. Sternlicht H, Rheinheimer W, Mehlmann A, Rothschild A, Hoffmann MJ, Kaplan WD. 2020. The mechanism of grain growth at general grain boundaries in $SrTiO_3$. *Scr. Mater.* 188:206–11
66. Sternlicht H, Rheinheimer W, Dunin-Borkowski RE, Hoffmann MJ, Kaplan WD. 2019. Characterization of grain boundary disconnections in $SrTiO_3$ part I: the dislocation component of grain boundary disconnections. *J. Mater. Sci.* 54:3694–709
67. Sternlicht H, Rheinheimer W, Hoffmann MJ, Kaplan WD. 2016. The mechanism of grain boundary motion in $SrTiO_3$. *J. Mater. Sci.* 51:467–75
68. Smith CS. 1952. Grain shapes and other metallurgical applications of topology. In *Metal Interfaces*, pp. 65–133. Cleveland, OH: Am. Soc. Metals
69. Smith CS. 1964. Some elementary principles of polycrystalline microstructure. *Metall. Rev.* 9:1–48
70. Mullins WW. 1956. Two-dimensional motion of idealized grain boundaries. *J. Appl. Phys.* 27:900–4
71. Herring C. 1953. The use of classical macroscopic concepts in surface energy problems. In *Structure and Properties of Solid Surfaces; Proceedings of a Conference Arranged by the National Research Council and Held in September, 1952, in Lake Geneva, Wisconsin, USA*, ed. R Gomer, CS Smith, pp. 5–81. Chicago: Univ. Chicago Press
72. MacPherson RD, Srolovitz DJ. 2007. The von Neumann relation generalized to coarsening of three-dimensional microstructures. *Nature* 446:1053–55
73. Bhattacharya A, Shen YF, Hefferan CM, Li SF, Lind J, et al. 2019. Three-dimensional observations of grain volume changes during annealing of polycrystalline Ni. *Acta Mater.* 167:40–50
74. Patterson BR, DeHoff RT. 2021. Linear relationship between dV/dt and grain volume during grain growth. *Metall. Mater. Trans. A* 52:3849–59
75. Shen YF, Maddali S, Menasche D, Bhattacharya A, Rohrer GS, Suter RM. 2019. Importance of outliers: a three-dimensional study of coarsening in α-phase iron. *Phys. Rev. Mater.* 3:063611
76. Zhang J, Zhang Y, Ludwig W, Rowenhorst D, Voorhees PW, Poulsen HF. 2018. Three-dimensional grain growth in pure iron. Part I. Statistics on the grain level. *Acta Mater.* 156:76–85
77. Powers JD, Glaeser AM. 1998. Grain boundary migration in ceramics. *Interface Sci.* 6:23–39
78. Beladi H, Nuhfer NT, Rohrer GS. 2014. The five-parameter grain boundary character and energy distributions of a fully austenitic high-manganese steel using three dimensional data. *Acta Mater.* 70:281–89
79. Beladi H, Rohrer GS. 2013. The relative grain boundary area and energy distributions in a ferritic steel determined from three-dimensional electron backscatter diffraction maps. *Acta Mater.* 61:1404–12
80. Li J, Dillon SJ, Rohrer GS. 2009. Relative grain boundary area and energy distributions in nickel. *Acta Mater.* 57:4304–11

81. Saylor DM, Morawiec A, Rohrer GS. 2002. Distribution and energies of grain boundaries in magnesia as a function of five degrees of freedom. *J. Am. Ceram. Soc.* 85:3081–83
82. Olmsted DL, Foiles SM, Holm EA. 2009. Survey of computed grain boundary properties in face-centered cubic metals: I. Grain boundary energy. *Acta Mater.* 57:3694–703
83. Ratanaphan S, Olmsted DL, Bulatov VV, Holm EA, Rollett AD, Rohrer GS. 2015. Grain boundary energies in body-centered cubic metals. *Acta Mater.* 88:346–54
84. Bulatov VV, Reed BW, Kumar M. 2014. Grain boundary energy function for fcc metals. *Acta Mater.* 65:161–75
85. Sarochawikasit R, Wang C, Kumam P, Beladi H, Okita T, et al. 2021. Grain boundary energy function for alpha iron. *Materialia* 19:101186
86. Abdeljawad F, Foiles SM, Moore AP, Hinkle AR, Barr CM, et al. 2018. The role of the interface stiffness tensor on grain boundary dynamics. *Acta Mater.* 158:440–53
87. Moore RD, Beecroft T, Rohrer GS, Barr CM, Homer ER, et al. 2021. The grain boundary stiffness and its impact on equilibrium shapes and boundary migration: analysis of the $\Sigma 5$, 7, 9, and 11 boundaries in Ni. *Acta Mater.* 218:117220
88. Blixt KH, Hallberg H. 2022. Grain boundary stiffness based on phase field crystal simulations. *Mater. Lett.* 318:132178
89. Lin B, Jin Y, Hefferan CM, Li SF, Lind J, et al. 2015. Observation of annealing twin nucleation at triple lines in nickel during grain growth. *Acta Mater.* 99:63–68
90. Taylor JE. 1992. II—Mean curvature and weighted mean curvature. *Acta Metall. Mater.* 40:1475–85
91. Anderson MP, Grest GS, Srolovitz DJ. 1989. Computer-simulation of normal grain-growth in 3 dimensions. *Phil. Mag. B* 59:293–329
92. Upmanyu M, Srolovitz DJ, Shvindlerman LS, Gottstein G. 1999. Misorientation dependence of intrinsic grain boundary mobility: simulation and experiment. *Acta Mater.* 47:3901–14
93. Chen L-Q. 2002. Phase-field models for microstructural evolution. *Annu. Rev. Mater. Res.* 32:113–40
94. Moelans N. 2022. New phase-field model for polycrystalline systems with anisotropic grain boundary properties. *Mater. Des.* 217:110592
95. Merriman B, Bence JK, Osher SJ. 1994. Motion of multiple junctions: a level set approach. *J. Comp. Phys.* 112:334–63
96. Merriman B, Bence JK, Osher S. 1992. *Diffusion Generated Motion by Mean Curvature*. Los Angeles: Dep. Math., Univ. Calif.
97. Esedoglu S, Otto F. 2015. Threshold dynamics for networks with arbitrary surface tensions. *Comm. Pure Appl. Math.* 68:808–64
98. Kobayashi R, Warren JA, Carter WC. 2000. A continuum model of grain boundaries. *Phys. D Nonlinear Phenom.* 140:141–50
99. Admal NC, Segurado J, Marian J. 2019. A three-dimensional misorientation axis- and inclination-dependent Kobayashi–Warren–Carter grain boundary model. *J. Mech. Phys. Solids* 128:32–53
100. Krill CE, Chen LQ. 2002. Computer simulation of 3-D grain growth using a phase-field model. *Acta Mater.* 50:3057–73
101. Naghibzadeh SK, Walkington N, Dayal K. 2021. Surface growth in deformable solids using an Eulerian formulation. *J. Mech. Phys. Solids* 154:104499
102. Peng X, Bhattacharya A, Naghibzadeh SK, Kinderlehrer D, Suter R, et al. 2022. Comparison of simulated and measured grain volume changes during grain growth. *Phys. Rev. Mater.* 6:033402
103. Barmak K, Eggeling E, Kinderlehrer D, Sharp R, Ta'asan S, et al. 2013. Grain growth and the puzzle of its stagnation in thin films: the curious tale of a tail and an ear. *Prog. Mater. Sci.* 58:987–1055
104. Demirel MC, Kuprat AP, George DC, Rollett AD. 2003. Bridging simulations and experiments in microstructure evolution. *Phys. Rev. Lett.* 90:016106
105. Gruber J, George DC, Kuprat AP, Rohrer GS, Rollett AD. 2005. Effect of anisotropic grain boundary properties on grain boundary plane distributions during grain growth. *Scr. Mater.* 53:351–55
106. Gruber J, Miller HM, Hoffmann TD, Rohrer GS, Rollett AD. 2009. Misorientation texture development during grain growth. Part I: simulation and experiment. *Acta Mater.* 57:6102–12

107. Salama H, Kundin J, Shchyglo O, Mohles V, Marquardt K, Steinbach I. 2020. Role of inclination dependence of grain boundary energy on the microstructure evolution during grain growth. *Acta Mater*. 188:641–51
108. Esedoglu S, Jacobs M, Zhang PB. 2017. Kernels with prescribed surface tension & mobility for threshold dynamics schemes. *J. Comp. Phys.* 337:62–83
109. Guziewski M, Zapiain DMD, Dingreville R, Coleman SP. 2021. Microscopic and macroscopic characterization of grain boundary energy and strength in silicon carbide via machine-learning techniques. *ACS Appl. Mater. Interfaces* 13:3311–24
110. Zhu Q, Samanta A, Li BX, Rudd RE, Frolov T. 2018. Predicting phase behavior of grain boundaries with evolutionary search and machine learning. *Nat. Comm.* 9:467
111. Dillon SJ, Rohrer GS. 2009. Mechanism for the development of anisotropic grain boundary character distributions during normal grain growth. *Acta Mater*. 57:1–7
112. Gottstein G, Molodov DA, Shvindlerman LS, Srolovitz DJ, Winning M. 2001. Grain boundary migration: misorientation dependence. *Curr. Opin. Solid State Mater. Sci.* 5:9–14
113. Winning M, Gottstein G, Shvindlerman LS. 2002. On the mechanisms of grain boundary migration. *Acta Mater*. 50:353–63
114. Winning M, Rollett AD, Gottstein G, Srolovitz DJ, Lim A, Shvindlerman LS. 2010. Mobility of low-angle grain boundaries in pure metals. *Phil. Mag.* 90:3107–28
115. Sun RC, Bauer CL. 1970. Tilt boundary migration in NaCl bicrystals. *Acta Metall.* 18:639–47
116. Gunster C, Molodov DA, Gottstein G. 2013. Migration of grain boundaries in Zn. *Acta Mater*. 61:2363–75
117. Furtkamp M, Gottstein G, Molodov DA, Semenov VN, Shvindlerman LS. 1998. Grain boundary migration in Fe–3.5% Si bicrystals with [001] tilt boundaries. *Acta Mater*. 46:4103–10
118. Viswanathan R, Bauer CL. 1973. Kinetics of grain-boundary migration in copper bicrystals with [001] rotation axes. *Acta Metall.* 21:1099–109
119. Molodov DA, Gunster C, Gottstein G, Shvindlerman LS. 2012. A novel experimental approach to determine the absolute grain boundary energy. *Phil. Mag.* 92:4588–98
120. Trenkle A, Syha M, Rheinheimer W, Callahan PG, Nguyen L, et al. 2020. Nondestructive evaluation of 3D microstructure evolution in strontium titanate. *J. Appl. Cryst.* 53:349–59
121. Patterson BR, DeHoff RT, Sahi CA, Sun J, Oddershede J, et al. 2019. *Integral mean curvature analysis of 3D grain growth: linearity of dV/dt and grain volume*. Paper presented at the 40th Risø International Symposium on Materials Science: Metal Microstructures in 2D, 3D and 4D, Roskilde, Denmark
122. Dake JM, Oddershede J, Sorensen HO, Werz T, Shatto JC, et al. 2016. Direct observation of grain rotations during coarsening of a semisolid Al–Cu alloy. *PNAS* 113: E5998–6006
123. Dake JM. 2019. *Experimental investigations of microstructural coarsening in 3D using X-ray microscopy*. PhD Diss., Univ. Ulm, Ulm, Ger.

Annual Review of Materials Research

Volume 53, 2023

Contents

Indexes

Errata

An online log of corrections to *Annual Review of Materials Research* articles may be found at http://www.annualreviews.org/errata/matsci